Available online at www.sciencedirect.com
ScienceDirect
Applied Acoustics 69 (2008) 614–623
applied acoustics
www.elsevier.com/locate/apacoust

Mechanisms of active control of sound transmission through a linked double-wall system into an acoustic cavity

Y.Y. Li [a,b], L. Cheng [a,*]

[a] Department of Mechanical Engineering, The Hong Kong Polytechnic University, Hung Hom, Kowloon, HKSAR, China
[b] Department of Mechanical and Automation Engineering, The Chinese University of Hong Kong, Shatin, N.W., HKSAR, China

Received 7 August 2006; received in revised form 9 November 2006; accepted 5 February 2007
Available online 26 March 2007

Abstract

The mechanism of active control on sound transmission through a mechanically linked double-wall structure into an acoustic cavity is investigated in this paper. Two control methods, i.e., structural control and acoustic control under two linkage cases (soft and hard) are investigated to analyze the effect of the links on the selection of control strategies and the corresponding control mechanisms. Simulations are performed to examine the dominant control mechanism (modal suppression or modal rearrangement) in different frequency ranges for each control case. The alteration in the structural-acoustic coupling is also analyzed so as to explain the mechanisms of sound attenuation. In addition, the dominance of the acoustic mode (0,0,0) in the energy transmission process as well as its use in designing a more effective sensor/actuator arrangement is discussed.

Keywords: Active noise control; Double-wall structure; Mechanical links; Transmission mechanism

1. Introduction

Noise control inside a cavity is a typical problem with great application potential in both industry and civil engineering. To control the interior noise, double-wall structures are widely used in mobile vehicles, partition walls in building and aircraft fuselage shells thanks to their superior noise insulation performance over single-leaf structures. This performance, however, deteriorates at low-frequencies due to the resonances of the air gap between the two walls. As an alternative to passive control, active control techniques have been explored to increase the noise transmission loss of double-wall structures in the low-frequency range [1–12]. Typical control strategies include acoustic control using acoustic sources, vibration control using structural actuators and isolation control.

Among double-wall systems, one configuration being extensively used is a double-wall structure radiating sound into a rectangular acoustic enclosure [13–15]. Pan et al. presented a theoretical model for active control of sound transmission through double-panels, in which three different control arrangements were investigated [13]. Using control loudspeakers inside the air gap, De Fonseca et al. experimentally demonstrated that an active sound transmission reduction could be achieved by reducing energy transmission through the gap [14].

In many practical situations, however, double-wall structures contain mechanical links to connect the two walls, which alter the energy transmission path. Apart from the acoustic transmitting path through the air gap between the two walls, energy can also be transmitted from the links, such forming a structural transmitting path. As a result, the inherent coupling between the panels and the cavities (the air gap and the enclosure) significantly increases the degree of complexity in terms of control. An example was from the experimental work of Bao et al. [16], which showed that the existence of the structural transmitting path could result in a change in both sensing arrangement and actuation mechanism or even jeopardize the success of the existing control

* Corresponding author. Tel.: +852 27666769; fax: +852 23654703.
E-mail address: mmlcheng@polyu.edu.hk (L. Cheng).

0003-682X/$ - see front matter © 2007 Elsevier Ltd. All rights reserved.
doi:10.1016/j.apacoust.2007.02.001

Nomenclature

c_0	sound speed of the air
C_m	rotational stiffness of the mechanical link
e_ℓ	blocked force per unit voltage of the actuator
F_{con}	control force applied between the two panels
$\boldsymbol{F}_{11}$,$\boldsymbol{F}_3$	generalized exciting pressure of $\widetilde{P}$ and generalized control pressure of P_{con}
$\boldsymbol{F}_{12}$, $\boldsymbol{F}_2$	generalized control forces
f_m	force produced by the mechanical link
K_m	translational stiffness of the mechanical link
K_g	aerostatic stiffness of the air gap
K, m_ℓ	stiffness and mass of the actuator
l_x, l_y, h_a	size lengths of panel a
L_p, L_{pg}	total acoustic potential energy inside the enclosure and the gap cavity
L_w	total-averaged kinetic energy received by the panel b
M, N	orders of mode to be truncated
M_x, M_y	rotational moments of the mechanical link
$m_{a,kl}, \zeta_{a,kl}$	generalized mass and modal damping of the klth mode of panel a
$\mathbf{n}$	the positive outward normal component
$\widetilde{P}$	acoustic excitation
P_g, P_{con}	sound pressure and control pressure inside the air gap
$\mathsf{P}_e, \mathsf{P}_g$	modal amplitudes of the enclosure and the air gap
$\widetilde{P}_\ell$	strength of control source inside the air gap
V	control voltage
V_g, V_e	volumes of the air gap cavity and the acoustic enclosure
w_a, D_a	transverse displacement and flexible rigidity of panel a
w_b, W_b	transverse displacement and modal amplitudes of panel b
δ	δ function
θ_x, θ_y	angular rotations of mechanical links
$\varphi_{kl}, q_{a,kl}$	mode shape functions and the corresponding modal coordinates of panel a
$\psi_{g,j}$	acoustic mode shapes of gap cavity
ρ_a, ρ	density of panel a and the air
$\omega_{g,j}, L^g_{j,kl}$	the jth angular frequency and modal coupling coefficient of gap cavity
$m_{g,jj}, \zeta_{g,j}$	the jth generalized mass and modal loss of gap cavity

strategies. Respective effects of the air gap and mechanical links on the energy transmission and noise insulation properties have been recently investigated in our previous work [17]. It was observed that the stiffness of the mechanical link and the aerostatic stiffness of the air gap are the two governing parameters controlling the energy transmission process. A criterion was then proposed to predict the dominant transmitting path and three different zones were identified. However, possible correlations between the dominant transmitting path and the most suitable control strategy for achieving an effective control remain unknown. An intuitive observation is that when the acoustic transmitting path is dominant, acoustic treatment may be a natural choice; whereas when the structural transmitting path is dominant, effort might be put on reducing structural energy transmission. So far, however, there exists no systematic analysis (theoretical or numerical) on this issue and subsequently on the corresponding control mechanism.

In this paper, we attempt to bring some answers to the above problems. It is pertinent to point out that this study does not intend to develop any novel modeling method or control algorithms. Instead, it rather puts emphasis on the physical phenomena related to the double-wall structures with mechanical links which will impact on the choice of control strategies. The paper is organized as follows. Firstly, a brief description on the modeling of the coupled vibro-acoustic system is given. Two different control strategies based on optimal control theory are examined: (a) acoustic control using loudspeakers inside the air gap and (b) structural control using structural actuators between the two panels. Numerical analyses are carried out to describe the effect of the sound transmitting paths on the selection of control strategies. Dominant control mechanisms in the low- and high-frequency ranges are examined so as to gain insight into the underlying physics. Finally, some conclusions are drawn.

2. Formulation

2.1. Vibro-acoustic model

The system under study is a double-wall structure coupled to an acoustic enclosure V_e shown in Fig. 1. The two panels, i.e., the incident panel a and the radiating panel b, are connected by a mechanical link at (x_m, y_m) and separated by an air gap cavity V_g. Apart from the surfaces occupied by these two panels, all other walls of both the air gap and the enclosure are acoustically rigid.

The modeling of the system using modal approach has been well documented in [7,17,18] and only a brief description is presented hereafter. For the panel a subjected to an acoustic excitation $\widetilde{P}$, the equation of motion is described as

$$\begin{aligned} D_a\nabla^4 w_a + \rho_a h_a \frac{\partial^2 w_a}{\partial t^2} = {} & \widetilde{P} - f_m \cdot \delta(x - x_m, y - y_m) - P_g(z = h_g) \\ & - F_{con} - M_x \cdot \delta(x - x_m)\delta'(y - y_m) \\ & - M_y \cdot \delta'(x - x_m)\delta(y - y_m) \end{aligned} \quad (1)$$

where w_a, D_a, ρ_a and h_a are the transverse displacement (positive downwards), the flexible rigidity, the density and the thickness of panel a; P_g the sound pressures inside

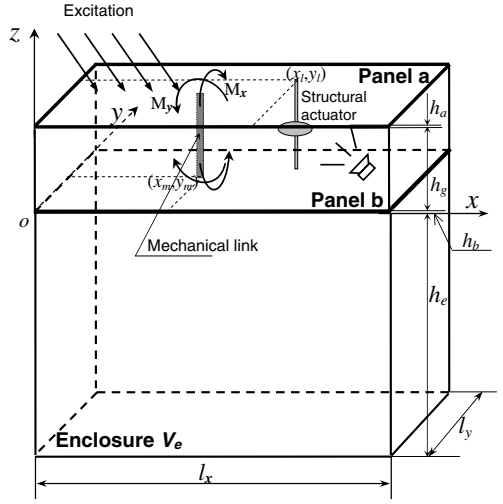

Fig. 1. An acoustic cavity covered with a linked double-wall structure.

the air gap; F_{con} the control force applied between the two panels; f_{m} and (M_x, M_y) the force and the rotational moments about the x- and y-axis produced by the mechanical link, which is simulated by a spring with a translational stiffness K_{m} and a rotational stiffness C_{m} as

$$f_{\text{m}} = K_{\text{m}}[w_{\text{a}}(x_{\text{m}}, y_{\text{m}}) - w_{\text{b}}(x_{\text{m}}, y_{\text{m}})], \quad M_x = C_{\text{m}}\theta_x, \quad M_y = C_{\text{m}}\theta_y, \tag{2}$$

where w_{b} is the transverse displacement of panel b, and (θ_x, θ_y) the angular rotations.

In general, w_{a} can be decomposed by the mode shape functions $\varphi_{kl}(x,y)$ and the corresponding modal coordinates $q_{\text{a},kl}(t)$ as $w_{\text{a}} = \sum_k \sum_l \varphi_{kl}(x,y) q_{\text{a},kl}(t)$. Substituting w_{a} into Eq. (1) and taking into account the viscous damping terms, one has

$$\begin{aligned}
&\ddot{q}_{\text{a},kl}(t) + 2\zeta_{\text{a},kl}\omega_{\text{a},kl}\dot{q}_{\text{a},kl}(t) + \omega^2_{\text{a},kl} q_{\text{a},kl}(t) \\
&= \frac{1}{m_{\text{a},kl}} \left\{ \int\int (\widetilde{P} - P_{\text{g}})\varphi_{kl}\,\mathrm{d}s - f_{\text{m}}\varphi_{kl}(x_{\text{m}}, y_{\text{m}}) \right. \\
&\quad - \int\int F_{\text{con}}\varphi_{kl}\,\mathrm{d}s - \int\int M_x \cdot \delta(x - x_{\text{m}})\delta'(y - y_{\text{m}})\varphi_{kl}\,\mathrm{d}s \\
&\quad \left. - \int\int M_y \cdot \delta'(x - x_{\text{m}})\delta(y - y_{\text{m}})\varphi_{kl}\,\mathrm{d}s \right\}, \mathrm{d}s = \mathrm{d}x\,\mathrm{d}y, \\
&k = 1, \ldots, \mathsf{M}; \quad l = 1, \ldots, \mathsf{N}
\end{aligned} \tag{3}$$

in which $m_{\text{a},kl}$ and $\zeta_{\text{a},kl}$ are the generalized mass and the modal damping of the klth mode, respectively, (M, N) the orders of mode to be truncated. Similarly, for the panel b,

$$\begin{aligned}
&\ddot{q}_{\text{b},kl}(t) + 2\zeta_{\text{b},kl}\omega_{\text{b},kl}\dot{q}_{\text{b},kl}(t) + \omega^2_{\text{b},kl} q_{\text{b},kl}(t) \\
&= \frac{1}{m_{\text{b},kl}} \left\{ f_{\text{m}}\varphi_{kl}(x_{\text{m}}, y_{\text{m}}) + \int\int F_{\text{con}}\varphi_{kl}\,\mathrm{d}s + \int\int (P_{\text{g}} - P_{\text{e}})\varphi_{kl}\,\mathrm{d}s \right. \\
&\quad + \int\int M_x \cdot \delta(x - x_{\text{m}})\delta'(y - y_{\text{m}})\varphi_{kl}\,\mathrm{d}s \\
&\quad \left. + \int\int M_y \cdot \delta'(x - x_{\text{m}})\delta(y - y_{\text{m}})\varphi_{kl}\,\mathrm{d}s \right\}.
\end{aligned} \tag{4}$$

For the air gap, the pressure inside the gap cavity is governed by the acoustic wave equation

$$\nabla^2 P_{\text{g}}(\mathbf{r}, t) - \frac{1}{c_0^2}\frac{\partial^2 P_{\text{g}}(\mathbf{r}, t)}{\partial t^2} = P_{\text{con}}, \tag{5a}$$

with boundary conditions

$$\frac{\partial P_{\text{g}}(\mathbf{r}, t)}{\partial \mathbf{n}} = \begin{cases} \rho\ddot{w}_{\text{a}} & \text{on panel a} \\ -\rho\ddot{w}_{\text{b}} & \text{on panel b} \\ 0 & \text{on the rigid wall} \end{cases} \tag{5b}$$

where ρ and c_0 are the density and sound speed of the air, respectively. P_{con} is the control pressure generated by sound sources inside the air gap. $\mathbf{n}$ is the positive outward normal component. Decomposing $P_{\text{g}}(\mathbf{r}, t)$ on the basis of acoustic mode shapes $\psi_{\text{g},j}(\mathbf{r})$ as $P_{\text{g}}(\mathbf{r}, t) = \sum_{j=1}^{n} \psi_{\text{g},j}(\mathbf{r}) p_{\text{g},j}(t)$, and using the Green's theorem, Eq. (5a) with the consideration of the viscous damping can be rewritten in a set of modal acoustic equations as follows:

$$\begin{aligned}
&\ddot{p}_{\text{g},j}(t) + 2\zeta_{\text{g},j}\omega_{\text{g},j}\dot{p}_{\text{g},j}(t) + \omega^2_{\text{g},j} p_{\text{g},j}(t) \\
&= \frac{c_0^2}{m_{\text{g},jj} V_{\text{g}}} \left[-\int P_{\text{con}}\psi_{\text{g},j}(\mathbf{r})\,dr \right. \\
&\quad \left. + \rho S \sum_k \sum_l L^{\text{g}}_{j,kl}(\ddot{q}_{\text{a},kl}(t) - \ddot{q}_{\text{b},kl}(t)) \right], \\
&S = l_x \times l_y, \ j = 1, \ldots, n
\end{aligned} \tag{6}$$

where $\omega_{\text{g},j}$, $m_{\text{g},jj}$, $\zeta_{\text{g},j}$ and $L^{\text{g}}_{j,kl}$ are the jth angular frequency, the generalized mass, the modal loss factor and the modal coupling coefficient, respectively. Similarly, for the enclosure,

$$\begin{aligned}
&\ddot{p}_{e,j}(t) + 2\zeta_{\text{e},j}\omega_{\text{e},j}\dot{p}_{\text{e},j}(t) + \omega^2_{\text{e},j} p_{\text{e},j}(t) \\
&= \frac{\rho c_0^2 S}{m_{\text{e},jj} V_{\text{e}}} \sum_k \sum_l L^{e}_{j,kl}\ddot{q}_{\text{b},kl}(t), \quad j = 1, \ldots, n_{\text{e}}.
\end{aligned} \tag{7}$$

In Eq. (7), all quantities with a subscript "e" are with the same meanings as defined for the gap cavity but apply to the enclosure. In the case of harmonic excitation, Eqs. (3), (4), (6) and (7) are reconstructed into a matrix form as

$$[\mathbf{H}] \begin{Bmatrix} \boldsymbol{A} \\ \boldsymbol{B} \\ \boldsymbol{C} \\ \boldsymbol{D} \end{Bmatrix} = \begin{Bmatrix} \boldsymbol{F}_{11} - \boldsymbol{F}_{12} \\ \boldsymbol{F}_2 \\ \boldsymbol{F}_3 \\ \mathbf{0} \end{Bmatrix}, \tag{8}$$

in which $\mathbf{H}$ describes the dynamic behaviors of the panels, the cavities and their interaction, while F_{11} the generalized exciting pressure (see Appendix). $(\boldsymbol{F}_{12}, \boldsymbol{F}_2)$ and $\boldsymbol{F}_3$ relate to the control voltage V or control pressure P_{con} to be optimized. Clearly, Eq. (8) describes the vibro-acoustic behavior of the coupled system with control actions, which will be solved to calculate coefficients $(\boldsymbol{A}, \ldots, \boldsymbol{D})$ for constructing the displacement of each panel and the acoustic pressure inside the cavity as

$$\begin{Bmatrix} \boldsymbol{A} \\ \boldsymbol{B} \\ \boldsymbol{C} \\ \boldsymbol{D} \end{Bmatrix} = [\mathbf{H}]^{-1} \begin{Bmatrix} \boldsymbol{F}_{11} - \boldsymbol{F}_{12} \\ \boldsymbol{F}_2 \\ \boldsymbol{F}_3 \\ \mathbf{0} \end{Bmatrix} = \begin{bmatrix} \cdots & \cdots & \cdots & \cdots \\ \boldsymbol{G}_{41} & \boldsymbol{G}_{42} & \boldsymbol{G}_{43} & \boldsymbol{G}_{44} \end{bmatrix} \begin{Bmatrix} \boldsymbol{F}_{11} - \boldsymbol{F}_{12} \\ \boldsymbol{F}_2 \\ \boldsymbol{F}_3 \\ \mathbf{0} \end{Bmatrix}. \tag{8a}$$

2.2. Active noise control

In light of our previous results [17,18], the stiffness of the mechanical link, K_m (or C_m), and the aerostatic stiffness of the air gap, K_g, are critical parameters for energy transmission. Depending on the ratio between K_m (or C_m) and K_g, three zones are identified to predict the dominant energy transmission path, i.e., from the air gap, the link or both blended. Since the translational effect on energy transmission is greater at low-frequencies compared with the rotational effect [18], only the translational effect on the selection of active control strategies will be considered. The optimal control is implemented to optimize the control input by defining the objective function as the total acoustic potential energy inside the enclosure [19]

$$L_p = \frac{1}{4\rho c_0^2} \int\int\int_{V_e} \mathsf{P}_e^*(\mathbf{r}) \mathsf{P}_e(\mathbf{r}) dv, \tag{9}$$

where

$$\mathsf{P}_e(\mathbf{r}) = \Psi_e(\mathbf{r})\boldsymbol{D}, \quad \Psi_e(\mathbf{r}) = [\psi_{e,1}, \ldots, \psi_{e,n_e}], \tag{9a, b}$$

$$\boldsymbol{D} = \boldsymbol{G}_{41}(\boldsymbol{F}_{11} - \boldsymbol{F}_{12}) + \boldsymbol{G}_{42}\boldsymbol{F}_2 + \boldsymbol{G}_{43}\boldsymbol{F}_3. \tag{8a′}$$

Case 1. Acoustic control using loudspeakers

In this case, $\boldsymbol{F}_{12} = \boldsymbol{F}_2 = \mathbf{0}$. Using a loudspeaker inside the air gap as the control source, P_{con} can be expressed as

$$P_{con} = -\mathrm{j}\omega \widetilde{P}_\ell \mathrm{e}^{\mathrm{j}\omega t} \delta(\mathbf{r} - \mathbf{r}_\ell), \tag{10}$$

where $\widetilde{P}_\ell$ is the strength of control source inside the air gap. The objective function L_p is therefore minimized as

$$L_p = \frac{V_e}{32\rho c_0^2} \left\{ \boldsymbol{F}_{ex}^H \boldsymbol{F}_{ex} - \frac{(\boldsymbol{F}_{ex}^H \boldsymbol{F}_{ac})^2}{\boldsymbol{F}_{ac}^H \boldsymbol{F}_{ac}} \right\} \tag{11a}$$

with the optimal control pressure

$$\widetilde{\mathbf{P}}_\ell = -\frac{V_g}{\mathrm{j}\omega c_0^2} \cdot \frac{\boldsymbol{F}_{ex}^H \boldsymbol{F}_{ac}}{\boldsymbol{F}_{ac}^H \boldsymbol{F}_{ac}}, \tag{11b}$$

where

$$\boldsymbol{F}_{ex} = \boldsymbol{G}_{41}\boldsymbol{F}_{11}, \quad \boldsymbol{F}_{ac} = \boldsymbol{G}_{43}\Psi_g^{\mathrm{T}}(\mathbf{r}_\ell),$$
$$\Psi_g(\mathbf{r}_\ell) = [\psi_{g,1}(\mathbf{r}_\ell), \ldots, \psi_{g,n}(\mathbf{r}_\ell)].$$

Case 2. Structural control using structural actuators

The selection of structural actuators plays a crucial role in active control. In this paper, a structural actuator, which produces comparatively higher force and larger displacement compared to traditional actuators, is used to connect the two panels [20] at (x_ℓ, y_ℓ). The control force can be divided into two parts: an active force f_ℓ and an inertial force f_ℓ^g induced by the mass of the actuator, i.e.,

$$F_{con} = (f_\ell - f_\ell^g)\delta(x - x_\ell, y - y_\ell), \tag{12a}$$

where

$$f_\ell = K[w_a(x_\ell, y_\ell) - w_b(x_\ell, y_\ell)] + e_\ell V,$$
$$f_\ell^g = -m_\ell[\ddot{w}_a(x_\ell, y_\ell) - \ddot{w}_b(x_\ell, y_\ell)], \tag{12b, c}$$

in which K, m_ℓ and e_ℓ are the dynamic stiffness and the mass of the actuator and the blocked force per unit voltage of the actuator, respectively.

For structural control, $\boldsymbol{F}_3 = \mathbf{0}$ and a minimized L_p can therefore be achieved as

$$L_p = \frac{V_e}{32\rho c_0^2} \left\{ \boldsymbol{F}_{ex}^H \boldsymbol{F}_{ex} - \frac{(\boldsymbol{F}_{str}^H \boldsymbol{F}_{ex})^2}{\boldsymbol{F}_{str}^H \boldsymbol{F}_{str}} \right\}, \tag{13a}$$

under the optimal control voltage

$$V = -\frac{1}{e_\ell} \cdot \frac{\boldsymbol{F}_{ex}^H \boldsymbol{F}_{str}}{\boldsymbol{F}_{str}^H \boldsymbol{F}_{str}}. \tag{13b}$$

where

$$\boldsymbol{F}_{str} = [\boldsymbol{G}_{42} - \boldsymbol{G}_{41}]\Phi^{\mathrm{T}}(x_\ell, y_\ell),$$
$$\Phi(x_\ell, y_\ell) = [\varphi_{11}(x_\ell, y_\ell), \ldots, \varphi_{MN}(x_\ell, y_\ell)].$$

3. Numerical simulations

Simulations are conducted using a structure (Fig. 1) with dimensions shown in Table 1. In this configuration, the aerostatic stiffness of the air gap is $K_g \approx 3.5 \times 10^5$ N/m. The acoustic excitation is an oblique plane wave with sound pressure amplitude of 1Pa, an azimuth angle 60° and an elevation angle 30°. Unless otherwise stated, a mechanical link is located at $(0.4l_x, 0.4l_y)$ to connect two panels, and the actuator at $(0.3l_x, 0.4l_y)$ for structural control while the loudspeaker at $(0.3l_x, 0.4l_y, 0.3h_g)$ for acoustic control.

3.1. General analysis

In order to reveal the effect of the transmitting paths on the selection of the control strategies, the two aforemen-

Table 1
The geometric size and boundary condition of the specimen

	Incident panel	Radiating panel	Air gap	Enclosure
Material	Aluminum		–	
$l_x \times l_y$ (m^2)		2.15×0.78		
Height (m)	0.004	0.006	0.55	0.11
Boundary condition	Simply-supported		Rigid	
Loss factor	0.005		0.001	

tioned control strategies with a soft and a hard link are first investigated. For analysis purpose, the vibration of the radiating panel and the pressure inside the air gap are also examined by defining the total-averaged kinetic energy received by the panel b as

$$L_w = \frac{\omega^2 \rho_b h_b}{S} \int\int_S W_b^*(x,y) W_b(x,y)\, ds, \tag{14}$$

and the total acoustic potential energy inside the gap cavity as

$$L_{pg} = \frac{1}{4\rho c_0^2} \int\int\int_{Vg} P_g^*(\mathbf{r}) P_g(\mathbf{r})\, dv, \tag{15}$$

in which $W_b(x,y)$ and $P_g(\mathbf{r})$ are the modal amplitudes of the panel b and the air gap.

Case 1: A soft link with $K_m = 10^2$ N/m

In this case, $K_m/K_g = 0.003 < 0.1$, the energy is mostly transmitted acoustically [17]. Fig. 2(a) shows the total acoustic potential energy L_p inside the enclosure without and with control. The attenuation of L_p is significant after the deployment of either structural or acoustic control.

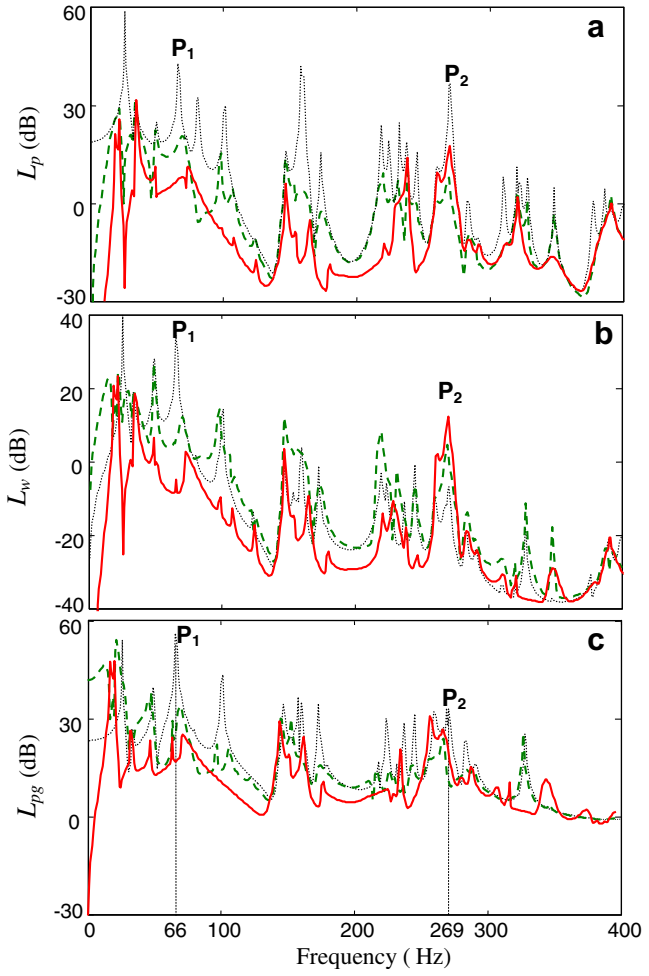

Fig. 2. System with a soft link; $K_m = 10^2$ N/m. (a) L_p inside the enclosure, (b) L_w of the radiating panel b, and (c) L_{pg} inside the air gap. ··· Uncontrolled; –– Structural control; — Acoustic control.

Comparison between the acoustic control (solid line) and the structural control (dashed) shows a more efficient control effect using the acoustic control scheme, especially in the low-frequency range. This phenomenon can be explained by examining the vibration of the radiating panel (L_w in Fig. 2(b)) and the pressure inside the air gap (L_{pg} in Fig. 2(c)). Due the dominance of the air gap in energy transmission, acoustic control weakens noise transmission through the air gap (Fig. 2(c)). As a result, the vibration of the radiating panel is suppressed (Fig. 2(b)) and the strength of pressure inside the enclosure is attenuated accordingly. This is true at low-frequencies, such as at $f = 66$ Hz (point p_1). With the increase of frequency, this tendency is, however, not maintained. Although L_p is still attenuated, this change does not fully come from the reduction of L_w. A typical example is the frequency region in the vicinity of $f = 269$ Hz (point p_2), in which L_w increases after control. Therefore, the reduction in L_p is not due to the suppression of the vibration level of the radiating panel. This observation suggests a possible change in modal coupling or modal rearrangement at these frequencies.

As far as structural control is concerned, the force generated by the actuator is not only applied to suppress the vibration of the radiating panel, but also exerted on the incident panel through the connection, resulting in a weakened sound transmission in the air gap (dotted line, Fig. 2(c)). Correspondingly, the energy in the enclosure is attenuated (dotted line, Fig. 2(a)). Based on the fact that the use of structural actuator cannot efficiently truncate the energy transmission path via the air gap, the control effect is limit compared with that obtained using a loudspeaker.

It is pertinent to mention that the phenomena observed in the low- and high-frequency ranges for acoustic control also apply to structural control, suggesting that there exist two control mechanisms at different frequency ranges, irrespective of the type of control strategies.

Case 2: *A hard link with* $K_m = 5 \times 10^6$ N/m

In this case, $K_m/K_g = 14.4 > 10$, the energy is mainly transmitted from the mechanical link [17]. Fig. 3(a)–(c) illustrate variations of L_p inside the enclosure, L_w received by the radiating panel and L_{pg} inside the air gap, respectively. Compared with the soft link case, a strong coupling between the two panels occurs with the increase of K_m, leading to a significant energy transmission through the link. Although both control strategies are effective for noise attenuation, acoustic control seems to be slightly better than structural control in the low-frequency range but worse in the high-frequency one. Once again, the phenomena observed at locations p_1 and p_2 in Fig. 2 with a soft link reoccur at the present case. That is, at p_1, acoustic control weakens noise transmission through the air gap, resulting in a vibration suppression of the radiating panel (L_w) and consequently an attenuation of the strength, L_p, of the pressure inside the enclosure; whereas at p_2, the reduction in L_p is not due to the suppression of L_w. It shows that the existence of two control mechanisms during the imple-

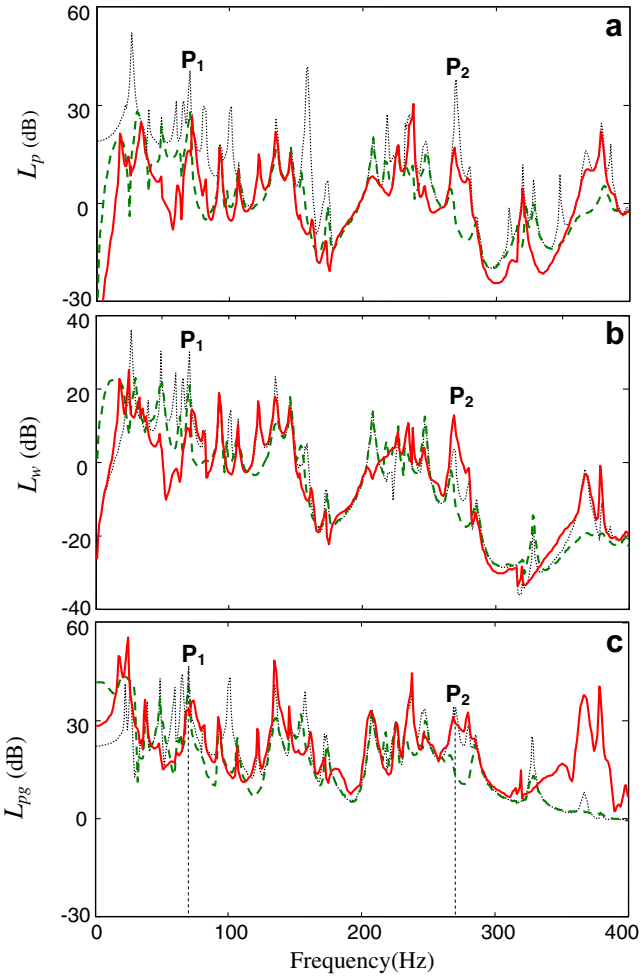

Fig. 3. System with a hard link; $K_m = 5 \times 10^6$ N/m. (a) L_p inside the enclosure, (b) L_w of the radiating panel b, and (c) L_{pg} inside the air gap.

mentation of optimal noise control, which is seemingly in agreement with that presented for a simple configuration [13,21–23]. In the following discussion, focus is put on analyzing the effect of control mechanisms on the design of control systems, e.g., the selection of actuators, and on structural-acoustic coupling.

3.2. Control strategies vs. energy transmission

The relationship between the selection of control strategies and energy transmission paths is investigated. An indicator γ describing this effect under different K_m/K_g is defined as

$$\gamma(K_m/K_g) = \frac{Area(L_p - L_p(\widetilde{P}_\ell, K_m/K_g))}{Area(L_p - L_p(\widetilde{P}_\ell, K_m/K_g)) + Area(L_p - L_p(V, K_m/K_g))} \times 100\%, \quad (16)$$

for acoustic control. $Area(\cdot)$ is the area under the spectrum concerned. A similar expression can be extended for structural control.

Fig. 4(a) shows the tendency of γ with an increasing K_m/K_g at the frequency band [0 400] Hz. It can be seen that in zone I, acoustic control is dominant because energy is thoroughly transmitted from the gap cavity; within zone II, structural control becomes effective with the increase of stiffness K_m due to the partial energy transmission through the link. Both strategies can be used for suppressing energy transmission when K_m/K_g falls into zone III corresponding to a very hard link. Fig. 4(b) depicts the variation of γ in the lower ([0 200] Hz) and higher ([201 400] Hz) frequency bands. It can be seen that structural control is superior to acoustic control at higher frequencies, while worse at lower one.

3.3. Control mechanisms

In order to deepen the understanding on the control mechanisms, analyses using *Case 1*, i.e., *a soft link with* $K_m = 10^2$ N/m at different frequencies are carried out. The vibration amplitude of the radiating panel at two representative frequencies, 56 Hz and 266 Hz, which are in the vicinity of P_1 and P_2, are plotted in Fig. 5(a) and (b), respectively. Focusing on the vibration patterns before and after control, it can be seen that at $f = 56$ Hz, both control strategies mainly reduce the vibration level of the panel without significantly changing the vibration pattern, in contrast with what happens at $f = 266$ Hz, for which the vibration pattern of the panel is modified remarkably under control actions. One possible reason is that at

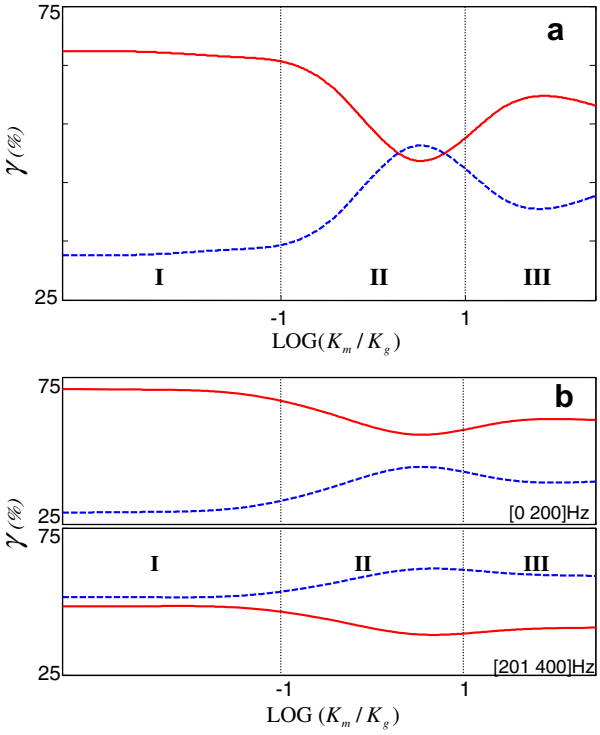

Fig. 4. Tendency of γ with an increasing K_m/K_g at frequency band: (a) [0 400] Hz and (b) [0 200] and [201 400] Hz. ––– Structural control; — Acoustic control.

$f = 266$ Hz, the vibration amplitude of the radiating panel is not only from a certain mode. Instead, it is a combination of several modes with different weightings. The deployment of the control changes these weightings, leading to a reconstruction of vibration pattern of the panel at this frequency. This alteration in the shape of the vibration certainly affects the coupling between the panel and the enclosure. The former mechanism can be regarded as modal suppression, whereas the latter is classified as modal rearrangement.

Revisiting Figs. 2 and 3 show that for both control strategies, modal suppression is the dominant control mechanism in the low-frequency range. In such case, sound reduction is a by-product of the vibration suppression in the radiating panel. Based on the fact that active control mainly targets low-frequencies, it is possible to attenuate the sound inside the enclosure by only using vibration sensors instead of acoustic sensors. This can significantly simplify the design and implementation of control systems, because in most cases, vibration sensors and actuators can be more easily embedded into the structures. An example is given in Fig. 6, which uses L_w as objective function instead of L_p. Obviously, L_p is attenuated together with a decrease in L_w in the low-frequency range. At high-frequencies, however, a reduction in L_w cannot result in a systematic reduction in L_p because of the dominance of modal rearrangement.

An understanding of the alteration in structural-acoustic coupling is realized by analyzing the effect of cavity modes inside the air gap on L_p and that of vibration modes on L_w. Fig. 7 illustrates the effect of acoustic modes on L_p for the structure with acoustic control. Before control (Fig. 7(a)), L_p at $f = 269$ Hz is contributed by the cavity mode $(2,1,0)$ ($f_{210} = 269$ Hz) and $(1,1,0)$ ($f_{110} = 232$ Hz) to a less extent. The influence of other modes is trivial. However, this situation is changed after control (Fig. 7(b)). That is, the dominance of mode $(2,1,0)$ on L_p is significantly weakened. Instead, the mode $(3,0,0)$ ($f_{300} = 237$Hz) becomes the most dominant, followed by the mode $(1,1,0)$. This change in the air gap subsequently affects the modal responses of the radiating panel, for which two modes $(1,1)$ and $(3,4)$ on L_w are plotted in Fig. 8. At $f = 269$ Hz, the mode $(3,4)$ is weakly excited before the control. After the control,

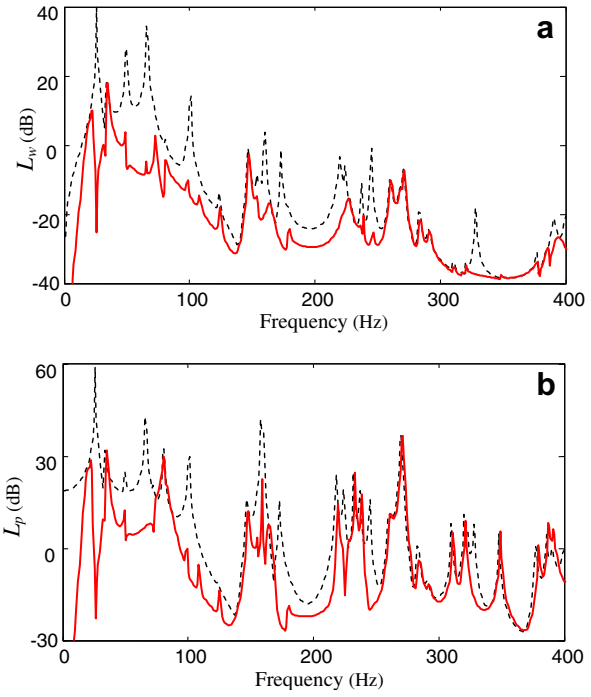

Fig. 6. Acoustic control with the optimization of the objective function L_w: (a) L_w of the radiating panel b and (b) L_p inside the enclosure. --- Uncontrolled; — Controlled.

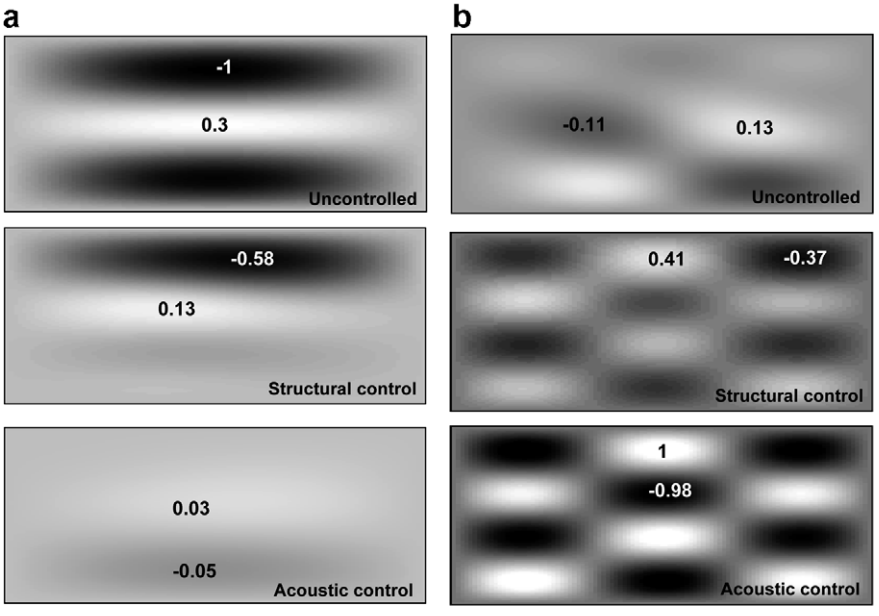

Fig. 5. Vibration pattern of the radiating panel b at (a) $f = 56$ Hz and (b) $f = 266$ Hz.

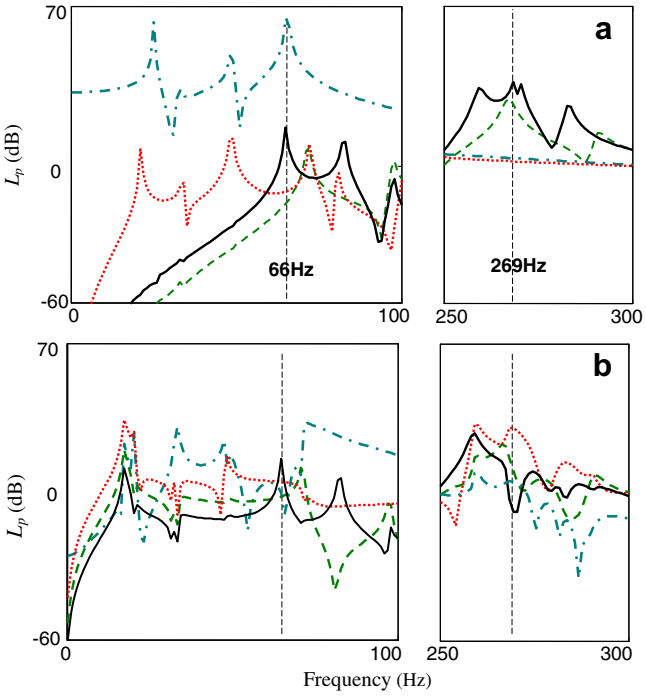

Fig. 7. Dominance of cavity modes on L_p. (a) Before control, and (b) After control. (0,0,0): ▬ ▪ ▪; (1,1,0): – – – ; (2,1,0): ——; (3,0,0): · · ·.

the response from this mode significantly increases, accompanied by a possible change in phase as well (not shown). This change in the modal response of the radiating panel will certainly affect its coupling with the enclosure. The above analysis does not apply to low-frequencies. At $f = 66$ Hz, for example, the dominant peak (mode (1, 1)) reduces after the control, showing the suppression mechanism at this frequency.

In light of Fig. 7(a), the cavity mode $(0,0,0)$ seems to play a dominant role on L_p in the low-frequency range for a soft link, in which the energy is mainly transmitted

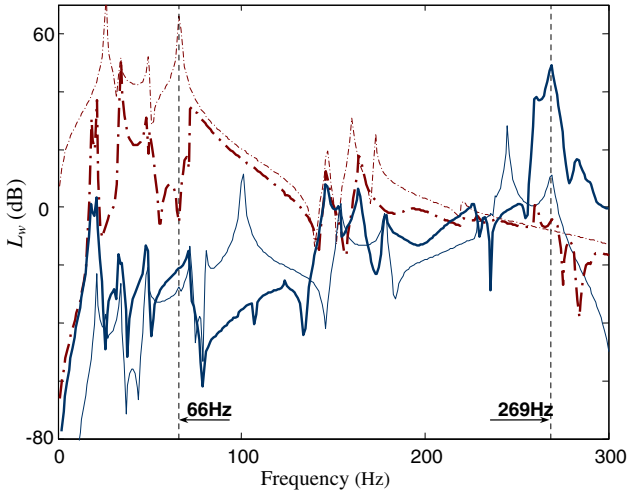

Fig. 8. Contribution of vibration modes on L_w. Mode (1,1): –·–·–·. Uncontrolled, ▬ ▪ ▬ Controlled; Mode (3,4): —— Uncontrolled, —— Controlled.

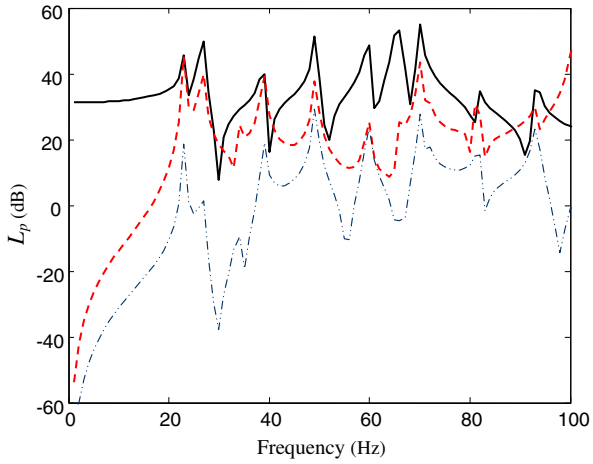

Fig. 9. Contribution of cavity modes on L_p for system with a hard link: $K_m = 5 \times 10^6$ N/m. (0,0,0): ——; (2,1,0): –··– ; (1,0,0): – – –.

from the acoustic path. Even for a hard link, the dominance of $(0,0,0)$ mode is still apparent, as shown in Fig. 9 for $K_m = 5 \times 10^6$ N/m.This observation suggests the use of any actuator arrangement would promote the response from $(0,0,0)$ mode inside the air gap during active control. In order to control low-frequency modes, a uniform control pressure field should be adopted rather than a point source, and synchronized multi-source actuation can provide a more homogeneous sound field without increasing the number of the control channels. As an example, Fig. 10 illustrates the effect of using (a) one control loudspeaker and (b) three synchronized control loudspeakers triangular-symmetrically located within the air gap. It can be seen that at low-frequencies, the synchronized multi-source actuation obviously outperforms the single-source control scheme, and the symmetric arrangement of sources can achieve a better control effect than the asymmetric cases. It is noticed that at a region controlled by

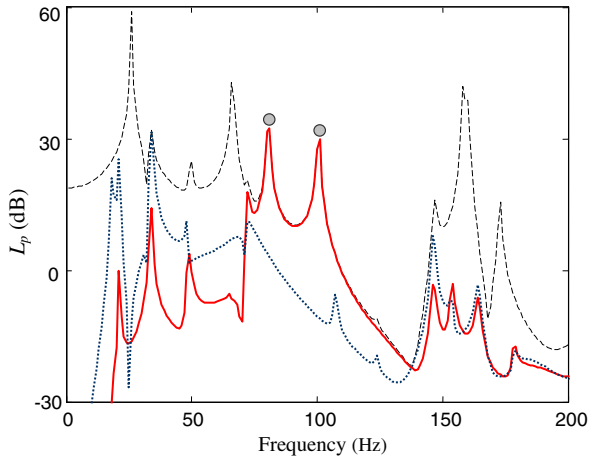

Fig. 10. Acoustic control: . . . . . a loudspeaker at $(0.3l_x, 0.3l_y, 0.3h_g)$; —— three synchronized loudspeakers triangular-symmetrically located at $(0.3l_x, 0.3l_y, 0.3h_g)$, $(0.5l_x, 0.7l_y, 0.3h_g)$ and $(0.7l_x, 0.3l_y, 0.3h_g)$; – – – without loudspeaker.

the frequencies 81 Hz and 101 Hz (marked with circles), no change in L_p can be observed using symmetrical arrangement of sources. The reason is that both two frequencies correspond to the acoustic mode $(1,0,0)$ of the enclosure and the structural mode $(1,2)$ of the radiating panel, symmetrical arrangement of the control sources has therefore no effect on modes.

4. Conclusions

Based on a fully coupled vibro-acoustic model, this paper investigates two control strategies for active control of noise transmission through a double-wall partition into an acoustic enclosure. Numerical simulations are performed to find the relationship between the control strategy, the transmission path and the control mechanism governing different frequency ranges. Results lead to the following conclusions:

(1) Dominant energy transmission path governs the selection of the control strategies. When the acoustic transmitting path is dominant, acoustic control can be adopted to attenuate the sound transmission.When the structural transmitting path is dominant, both structural and acoustic controls are effective for noise reduction. However, structural control seems to outperform acoustic control at higher frequencies while producing opposite effect at lower ones. In addition, two control mechanisms simultaneously exist for different control strategies. The dominance of the suppression mechanism can simplify the design of the control systems by only using vibration sensors instead of acoustic sensors.
(2) Acoustic mode $(0,0,0)$ inside the air gap dominates the energy transmission process at low-frequencies, such suggesting the use of those actuator arrangements which promote the response from $(0,0,0)$ mode for a better control. It is verified that the synchronized single-channel control with multi-control sources yields a better control result than a single-point source does, and the symmetric arrangement of control sources is more effective than the asymmetric ones.

Acknowledgements

The authors would like to thank the Research Committee of The Hong Kong Polytechnic University for the financial support to this project (G-U136 and G-U031). The second author wishes to acknowledge the support from a special fund for recently promoted Chair Professors given by The Hong Kong Polytechnic University.

Appendix

In Eq. 8,

$$\mathbf{H}=\begin{bmatrix} \boldsymbol{H}_{11} & \boldsymbol{H}_{12} & \boldsymbol{H}_{13} & \mathbf{0} \\ \boldsymbol{H}_{12}^{\mathrm{T}} & \boldsymbol{H}_{22} & \boldsymbol{H}_{23} & \boldsymbol{H}_{24} \\ \boldsymbol{H}_{31} & \boldsymbol{H}_{32} & \boldsymbol{H}_{33} & \mathbf{0} \\ \mathbf{0} & \boldsymbol{H}_{42} & \mathbf{0} & \boldsymbol{H}_{44} \end{bmatrix},$$

where

$$\begin{aligned}\boldsymbol{H}_{11} &= \boldsymbol{M}_{\mathrm{a}} + K_{\mathrm{m}}\boldsymbol{\Phi}^{\mathrm{T}}(x_{\mathrm{m}},y_{\mathrm{m}})\boldsymbol{\Phi}(x_{\mathrm{m}},y_{\mathrm{m}}) + (K_{\ell} \\ &\quad - m_0^{\ell}\omega^2)\boldsymbol{\Phi}^{\mathrm{T}}(x_{\ell},y_{\ell})\boldsymbol{\Phi}(x_{\ell},y_{\ell}) \\ &\quad + C_{\mathrm{m}}\left[\boldsymbol{\Theta}_x^{\mathrm{T}}(x_{\mathrm{m}},y_{\mathrm{m}})\boldsymbol{\Theta}_x(x_{\mathrm{m}},y_{\mathrm{m}}) - \boldsymbol{\Theta}_y^{\mathrm{T}}(x_{\mathrm{m}},y_{\mathrm{m}})\boldsymbol{\Theta}_y(x_{\mathrm{m}},y_{\mathrm{m}})\right],\end{aligned}$$

$$\begin{aligned}\boldsymbol{H}_{22} &= \boldsymbol{M}_{\mathrm{b}} + K_{\mathrm{m}}\boldsymbol{\Phi}^{\mathrm{T}}(x_{\mathrm{m}},y_{\mathrm{m}})\boldsymbol{\Phi}(x_{\mathrm{m}},y_{\mathrm{m}}) + (K_{\ell} \\ &\quad - m_0^{\ell}\omega^2)\boldsymbol{\Phi}^{\mathrm{T}}(x_{\ell},y_{\ell})\boldsymbol{\Phi}(x_{\ell},y_{\ell}) \\ &\quad + C_{\mathrm{m}}\left[\boldsymbol{\Theta}_x^{\mathrm{T}}(x_{\mathrm{m}},y_{\mathrm{m}})\boldsymbol{\Theta}_x(x_{\mathrm{m}},y_{\mathrm{m}}) - \boldsymbol{\Theta}_y^{\mathrm{T}}(x_{\mathrm{m}},y_{\mathrm{m}})\boldsymbol{\Theta}_y(x_{\mathrm{m}},y_{\mathrm{m}})\right],\end{aligned}$$

$$\boldsymbol{F}_{11} = \int_S \widetilde{P}(x,y)\boldsymbol{\Phi}^{\mathrm{T}}(x,y)\,\mathrm{d}s,$$

$$\boldsymbol{\Phi}(x,y) = [\varphi_{11}(x,y),\ldots,\varphi_{\mathsf{MN}}(x,y)],$$

$$\boldsymbol{\Theta}_x(x,y) = \frac{\partial\boldsymbol{\Phi}(x,y)}{\partial x}, \quad \boldsymbol{\Theta}_y(x,y) = \frac{\partial\boldsymbol{\Phi}(x,y)}{\partial y}.$$

The expressions of $\boldsymbol{M}_{\mathrm{a}}$, $\boldsymbol{M}_{\mathrm{b}}$, $\boldsymbol{H}_{12}$, $\boldsymbol{H}_{13}$, and $\boldsymbol{H}_{44}$ are the same as those presented in [17,18].

References

[1] Grosveld FW, Shepherd KP. Active sound-attenuation across a double-wall structure. J Aircraft 1994;31:223–7.
[2] Carneal JP, Fuller CR. Active structural acoustic control of noise transmission through double panel systems. AIAA J 1995;33:618–23.
[3] Bao C, Pan J. Experimental study of different approaches for active control of sound transmission through double walls. J Acoust Soc Am 1997;102:1664–70.
[4] Wang CY, Vaicaitis R. Active control of vibrations and noise of double wall cylindrical shells. J Sound Vib 1998;216:865–88.
[5] Pan X, Sutton TJ, Elliott SJ. Active control of sound transmission through a double-leaf partition by volume velocity cancellation. J Acoust Soc Am 1998;104:2828–35.
[6] Gardonio P, Elliott SJ. Active control of structure-borne and airborne sound transmission through double panel. J Aircraft 1999;36:1023–32.
[7] Kaiser OE, Pietrzko SJ, Morari M. Feedback control of sound transmission through a double glazed window. J Sound Vib 2003;263:775–95.
[8] Jakob A, Moser M. Active control of double-glazed windows – Part I: Feedforward control. Appl Acoust 2003;64:163–82.
[9] Jakob A, Moser M. Active control of double-glazed windows. Part II: Feedback control. Appl Acoust 2003;64:183–96.
[10] Carneal JP, Fuller CR. An analytical and experimental investigation of active structural acoustic control of noise transmission through double panel systems. J Sound Vib 2004;272:749–71.
[11] Mao QB, Pietrzko S. Control of sound transmission through double wall partitions using optimally tuned Helmholtz resonators. ACTA Acustica United with Acustica 2005;91:723–31.
[12] Paurobally R, Pan J , Bao C. Feedback control of noise transmission through a double-panel partition. In: Proceedings of Active 99, Fort Lauderdale, Florida, USA, 1999, p. 375–86.
[13] Pan J, Bao C. Analytical study of different approaches for active control of sound transmission through double walls. J Acoust Soc Am 1998;103:1916–22.

[14] De Fonseca P, Sas P, Van Brussel H. Experimental study of the active sound transmission reduction through a double panel test section. Acustica 1999;85:538–46.
[15] Sas P, Bao C, Augusztinovisz F, Desmet W. Active control of sound transmission through a double-panel partition. J Sound Vib 1995;180:609–25.
[16] Bao C, Pan J. Active acoustic control of noise transmission through double walls: effect of mechanical paths. J Sound Vib 1998;215:395–8.
[17] Cheng L, Li YY, Gao JX. Energy transmission in a mechanically-linked double-wall structure coupled to an acoustic enclosure. J Acoust Soc Am 2005;117:2742–51.
[18] Li YY, Cheng L. Energy transmission through a double-wall structure with an acoustic enclosure: Rotational effect of mechanical links. Appl Acoust 2006;67:185–200.
[19] Nelson PA, Elliott SJ. Active Control of Sound. London: Academic Press; 1993.
[20] Copeland BM, Buckley JD, Bryant RG, Fox RL, Hellbaum RF. An ultra-high displacement piezoelectric actuator. NASA Langley Research Center 1999. 23681-0001.
[21] Hagiwara I, Wang DW, Shi QZ, Rao RS. Reduction of noise inside a cavity by piezoelectric actuators. J Vib Acoust – Trans ASME 2003;125:12–7.
[22] Qiu XJ, Sha JZ, Yang J. Mechanisms of active control of noise transmission through a panel into a cavity using a point force actuator on the panel. J Sound Vib 1995;182:167–70.
[23] Sampath A, Balachandran B. Studies on performance functions for interior noise control. Smart Mater Struct 1997;6:315–32.